Supporting Information

Spin-Pair-State Induced Exceptional Magnetic Field Responses from Thermally Activated Delayed Fluorescence-Assisted Fluorescent Material Doping System

Yeqian Hu, Xiantong Tang, Ruiheng Pan, Jinqiu Deng, Hongqiang Zhu, and Zuhong Xiong*

School of Physical Science and Technology, MOE Key Laboratory on Luminescence and Real-Time Analysis, Southwest University, Chongqing 400715, People's Republic of China

E-mail: zhxiong@swu.edu.cn

1. Experimental Apparatus and Devices Structures

A schematic illustration of the experimental apparatus for measuring the MEL and MC results from devices used in this work is depicted in Fig.S1. During measurement, the samples were mounted on a cold finger of a closed-cycle cryostat (Janis CCS-350S) that was located between two poles of an electromagnet (Lakeshore EM4), which was powered by a Lakeshore EM647 unit. The measurements were performed at a pressure of ~10^{-2} Pa, which was controlled by a rotary pump (Edwards RV12). A Keithley 2400 SourceMeter was used to provide a constant voltage and measure the device current. The brightness of the devices was determined using a magnetic insensitive silicon photodetector that was connected to a brightness meter (ST-86LA) and a multimeter (Keithley 2000) and recorded on a computer. The external magnetic field (B) was measured by a Hall plate connected to a Gaussmeter (Lakeshore 421), and then recorded using a computer connected with this Gaussmeter through RS232 wire. The temperature was set using a temperature controller (Lakeshore 331). The EL and PL spectra were measured with a SpectraPro-2300i spectrometer with a laser excitation

wavelength of 325 nm for the PL measurements. The absorption spectra were recorded using a UV-VIS Spectrophotometer (UV-2600).

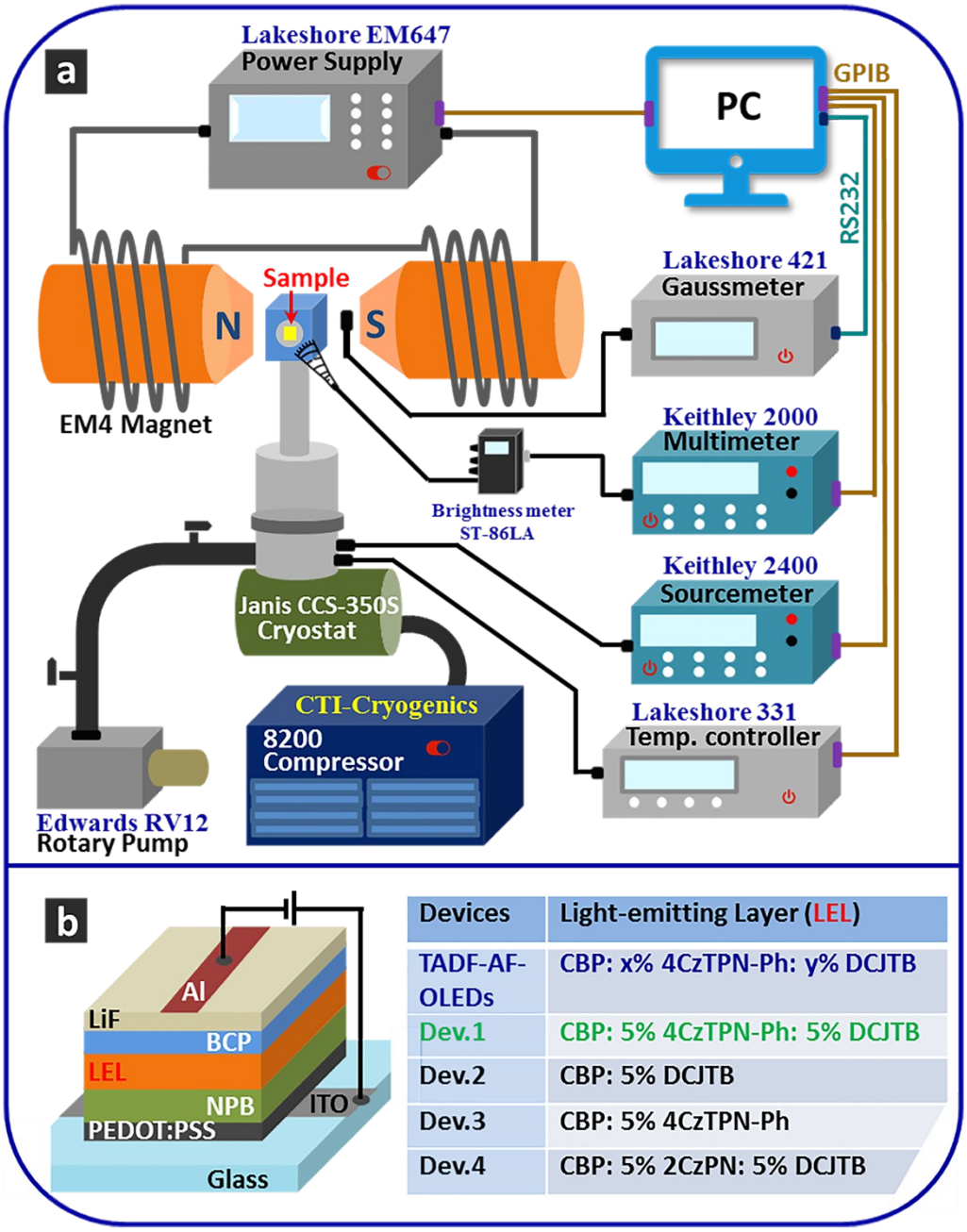

Fig. S1 Schematic illustration of experimental apparatus for measuring the MEL and MC of the TADF-AF-OLEDs. The device structure is also shown.

2. Theories of Spin-pair State Inter-conversions and Energy Transfer Process

The fingerprint MEL and MC curves caused by *B*-mediated ISC are shown by the blue

curve in Fig. 1d. Both MEL and MC increase sharply at low B ($|B|$<20 mT) and are saturated at high fields. The positive low-field magnetic response curve has a Lorentzian line shape with full width at half maximum (FWHM) from several mT up to ~20 mT,[1,2] which originates from B-suppressed hyperfine interactions between polaron pairs (including singlet PP_1 and triplet PP_3). That is, when the external field $B_{ext} = 0$, PP_1 can interconvert with PP_3 (including energetically degenerated PP_3^+, PP_3^0, and PP_3^-) because of hyperfine interactions between polarons and nuclear spins in an OLED, which is ISC between polaron pairs ($PP_1 \rightarrow PP_3$). When an external B_{ext} is applied, the PP_3^+, PP_3^0, and PP_3^- species are no longer degenerate because of Zeeman splitting, which leads to reduced ISC (only $PP_1 \rightarrow PP_3^0$ occurs) and in turn causes enhanced EL_B and I_B. Moreover, the hyperfine interaction field (B_{HF}) is less than 20 mT, and when $B_{ext} >> B_{HF}$, the suppression of ISC caused by the B_{ext} is not changed, which results in the saturation of the MEL and MC traces at high B. The differing spatial extensions of the wave-functions between polaron-pairs should result in the distinct FWHM within a certain magnetic field range (< ~20 mT),[1,2] which originates from B-suppressed ISC between different material polaron pairs. RISC between polaron pairs ($PP_3 \rightarrow PP_1$) is the opposite process to ISC, so its corresponding MEL and MC curves should be inverted in sign,[3,4] as illustrated by the purple curve shown in Fig. 1d. Moreover, the MEL and MC traces caused by RISC process between excitons ($T_1 \rightarrow S_1$) should be also anti-symmetry but with different FWHM as compared to the RISC of polaron pairs owing to the different spatial extension of wave-functions between excitons and polaron-pairs.[2]

TF, which can be expressed as $T_1+T_1 \rightarrow S_1+S_0$,[5] is affected by the external B because of Zeeman splitting of the triplet exciton. At low fields ($|B|$<20 mT), the B-induced Zeeman splitting is less than the zero-field splitting and so will enhance the rate of annihilation of triplet excitons (T_1), which causes the initial rise in the electroluminescence with increasing magnetic field. At high fields ($|B|$>20 mT), the B-induced Zeeman splitting is larger than zero-field splitting, which causes the annihilation rate to drop and in turn the MEL decreases.[6]

Therefore, TF causes a MEL trace like that shown by the green line in Fig. 1d.

The TQA scattering process proposed by Desai *et al.* involves triplet excitons (T) colliding with free carriers (Q),[7] which decreases carrier mobility ($T+Q\rightarrow T+Q'$) and reduces the current of device. An external B can suppress the rate of collision between T and Q, which causes a slowly increasing positive MC trace at low-fields with a non-Lorentzian line shape and a FWHM of ~100 mT, as shown by the red curve in Fig. 1d. Therefore, MEL and MC curves from simple systems typically display no more than two components, which can be used to understand the underlying mechanisms that occur within a device.

3. Absorption and Photoluminescence Spectra

The photoluminescence (PL) spectra of CBP, 4CzTPN-Ph, and 2CzPN and the absorption spectra of 4CzTPN-Ph and DCJTB are shown in Fig. S2. The energy transfer processes in OLED may involve several different processes, including direct charge trapping (DCT) as well as FRET and DET processes.[8-13] The overlap of absorption and emission spectra of the acceptor and the donor is a necessary sufficient condition for the FRET and DET process. And the FRET radius can be caculated by the donor PL spectrum and the acceptor absorption spectrum.

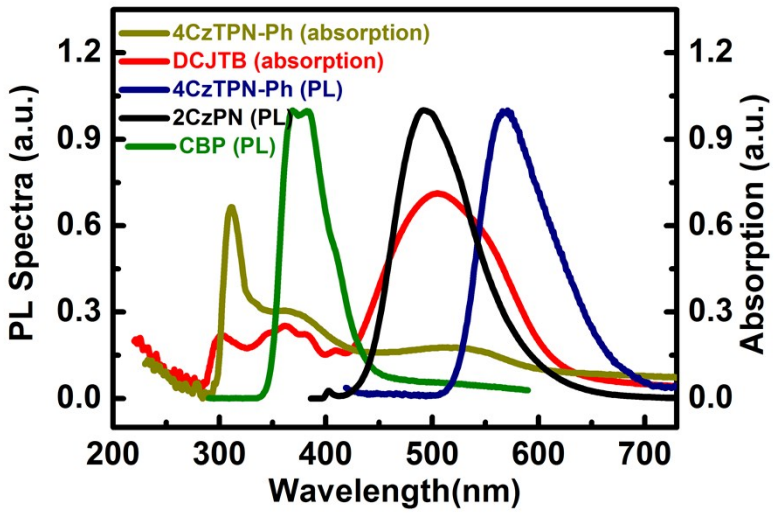

Fig. S2 Absorption and photoluminescence spectra of CBP, 4CzTPN-Ph, DCJTB and 2CzPN.

In Fig. S2, the absorption spectrum of 4CzTPN-Ph is composed of two peaks of 320 nm and 370 nm, which overlap with the PL spectrum (376 nm) of CBP. This situation meets the requirement of FRET and DET processes. The DCJTB absorption spectrum is peaked at 510 nm, which less overlaps with the PL spectrum of CBP. This means that the FRET process cannot occur between CBP and DCJTB molecules. Therefore, DCJTB is only likely to acquire energy via DCT process. The PL spectrum of 4CzTPN-Ph is peaked at 590 nm, and the absorption spectrum of DCJTB is peaked at 510 nm. That is, this PL spectrum of 4CzTPN-Ph overlaps partially with the absorption spectrum of DCJTB, indicating that the energy on 4CzTPN-Ph molecule is transferred to DCJTB via FRET or DET process. In order to further determine the energy transfer process among these materials, it is necessary to estimate the distance of the donor and acceptor. The specific analysis can be found in the main text.

Moreover, when 4CzTPN-Ph was replaced by the homogeneous material 2CzPN, which had a wider energy gap (see Fig. S5), the overlap between the PL spectrum of 2CzPN and the absorption spectrum of DCJTB was greater. Therefore, FRET between 2CzPN and DCJTB was stronger than between 4CzTPN-Ph and DCJTB, which led to enhanced spin-pair state inter-conversions (i.e. TF and RISC) in DCJTB.

4. MC Curves and Related EL and PL Spectra

Using the formula of $EL \propto \eta I$,[14,15] we can easily obtain the relationship of $MEL = M\eta + MC$, where η is the external quantum efficiency. This shows that MEL is a combination of both $M\eta$ and MC. In fact, MC can reflect the intrinsic properties of charge carrier transport.[16] Thus, we have measured and compared the MC results of Dev.1 (CBP:5%4CzTPN-Ph:5%DCJTB), Dev.2 (CBP:5%DCJTB), and Dev.3 (CBP:5%4CzTPN-Ph) after the behavior of their MEL was discussed in section 3.3 of main text. The MC curves of these devices within a large magnetic field range (300 mT), their normalized EL spectra, and the normalized PL spectra of

4CzTPN-Ph and DCJTB at room temperature are shown in Fig. S3. The MC behavior of Dev.1 and Dev.2 was similar, but was markedly different from Dev.3, especially the low-field MC components (Figs. S3a, S3b, and S3c, respectively). Specifically, the MC curves of Dev.1 and Dev.2 rise sharply at low field ($|B|$<20 mT) and then increase slowly at high field ($|B|$>20 mT). The low-field MC reflected the *B*-suppressed ISC of CBP polaron pairs,[17] while the high-field MC behavior was similar to the fingerprint trace caused by TQA (red line, Fig. 1d). This indicated that a TQA scattering process also existed in Dev.1 and Dev.2.[16] Obviously, it is plausible for Dev.1 and Dev.2 to have similar MC results because of their identical EL spectra that had peak emission wavelengths at 600 nm, as shown in Fig. S3d. This meant that the EL from both devices was originated from the radiative de-excitation of DCJTB. However, the EL from Dev.3 had a peak emission wavelength of 580 nm (orange line, Fig. S3d), which was the same as the PL of 4CzTPN-Ph. This indicated that the EL of Dev.3 was originated from the 4CzTPN-Ph guest molecules. Thus, different energy transfer processes and spin-pair state inter-conversions occurred in 4CzTPN-Ph and DCJTB led to the different MC results from Dev.3, when compared with Dev.1 and Dev.2.

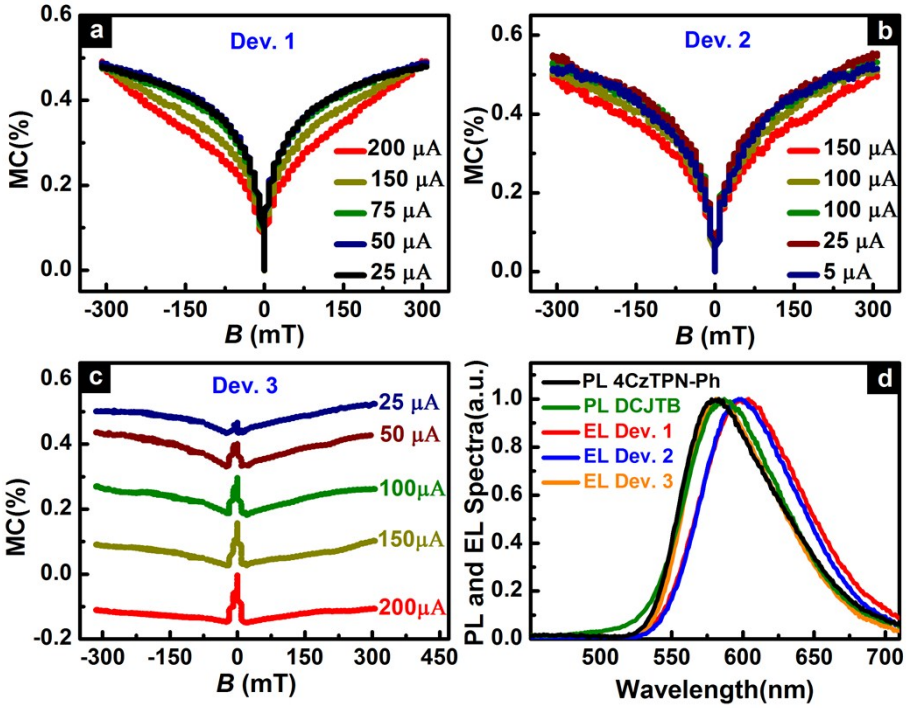

Fig. S3 Current-dependent MC(*B*) responses from the TADF-AF-OLEDs within a *B* of ±300 mT at room temperature (295 K). (a) Dev.1, CBP:5%4CzTPN-Ph:5%DCJTB. (b) Dev.2, CBP:5%DCJTB. (c) Dev.3, CBP:5%4CzTPN-Ph. (d) Normalized EL spectra of Dev.1, Dev.2 and Dev.3 and PL spectra of DCJTB and 4CzTPN-Ph in film. In order to clearly see the MC fine structure at the low field range in Fig. S3c, we fix the zero-field value of the MC trace acquired at 200 μA to be zero, and vertically shift the corresponding MC curves obtained at other currents (150 μA, 100 μA, 50 μA, and 25 μA) through adding some proper values (0.2%, 0.3%, 0.4%, and 0.5%) to their MC magnitudes, respectively. The shifts in other figures were made with similar ways.

In contrast to the positive low-field MC curves that were observed from Dev.1 and Dev.2, Dev.3 exhibited negative low-field MC components that decrease rapidly within small magnetic field strengths ($|B|<8$ mT), as shown in Fig. S3c. The low-field ($|B|<8$ mT) MC curve of Dev.3 was similar to the fingerprint trace caused by RISC (purple line, Fig. 1d), which was caused by RISC of 4CzTPN-Ph charge-transfer excitons. The high-field ($|B|>8$ mT) MC curves from Dev.3 shown in Fig. S3c were similar to the fingerprint trace that is caused by TQA (red line, Fig. 1d), which indicated that the TQA scattering process also existed in Dev.3. Intriguingly, the MEL curves of Dev.2 and Dev.3 exhibited negative and positive low-field responses but the MC curves of Dev.2 and Dev.3 showed positive and negative low-field responses, which were caused by spin-pair state inter-conversions that were influenced by the energy transfer processes occurred within the devices as explained in the section 3.3 of main text.

5. Temperature-Dependent MEL Curves from TADF-AF-OLEDs with Lager Field Range

Temperature-dependent MEL curves that were obtained over a large magnetic field range (300 mT), at small (20 μA) and large (150 μA) injection currents are shown in Fig. S4.

The MEL_H component ($|B|$>20 mT) is influenced by RISC of 4CzTPN-Ph charge-transfer excitons and TF of DCJTB excitons at ambient temperature. However, RISC is dominant at small currents and TF is dominant at large currents. As the temperature was lowered, the MEL_H component at an IC of 20 μA was weakened (Fig. S4a). This was caused by weakened RISC of 4CzTPN-Ph charge-transfer excitons, as discussed previously. However, the MEL_H component did not show significant changes with temperature at an IC of 150 μA (Fig. S4b). This result showed that the temperature did not have notable influence on the TF process of DCJTB excitons in Dev.1, which was consistent with the literature reports.[18]

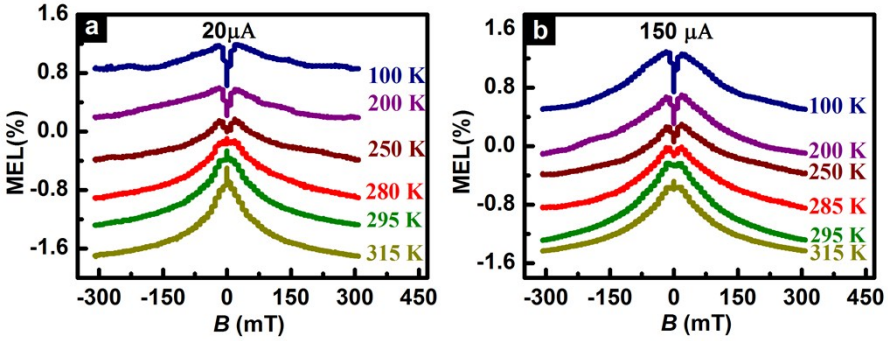

Fig. S4 (a), (b) Temperature-dependent MEL(B) response of Dev.1 within a B of ±300 mT at small (20 μA) and large (150 μA) injection currents, respectively. The MEL traces are also shifted via the same manners as those in Fig. S3 to clearly observe the low-field parts of MEL traces.

6. Influence of Dopant energy Gap of TADF-AF-OLED Behavior

The source of the EL emission from Dev.1 (CBP:5%4CzTPN-Ph:5% DCJTB) was DCJTB (Fig. S3d). Energy was initially transferred from CBP to 4CzTPN-Ph, which then transferred to DCJTB via FRET. To further probe the mechanisms that occurred in the devices, we replaced the sensitizer material (4CzTPN-Ph) in Dev.1 with a homogeneous material with a wider energy gap (2CzPN, E_{HOMO}=5.8 eV, E_{LUMO}=3.0 eV) to fabricate Dev.4 (ITO/PEDOT:PSS/NPB/CBP:5%2CzPN:5%DCJTB/BCP/LiF/Al, Fig. S5a). The EL spectrum of Dev.4 was almost identical to that of Dev.1 (Fig. S5b), which indicated that the EL

emissions from both Dev.4 and Dev.1 were originated from DCJTB. It can be seen from Fig.S2 that the overlap between the PL spectrum of 2CzPN and the absorption spectrum of DCJTB is relatively large as compared to the overlap between the PL spectrum of 4CzTPN-Ph and the absorption spectrum of DCJTB. Therefore, FRET process between 2CzPN and DCJTB should be more efficient than that between 4CzTPN-Ph and DCJTB. When 4CzTPN-Ph is replaced by 2CzPN, DCJTB will be easier to obtain energy from 2CzPN, which is beneficial to the formation of spin-pair-states inter-conversion process on DCJTB.

The room temperature MEL curves obtained from Dev.4 within ±300 mT and ±50 mT under different ICs are shown in Figs. S5c and S5d, respectively. The MEL_H components from Dev.4 (Fig. S5c) and Dev.1 (Fig. 4a) were similar to each other. That is, the declining MEL_H components at high ICs did not saturate at high field strength, but did at small ICs. Therefore, the MEL_H component of Dev.4 at high ICs was also determined by the TF of DCJTB excitons, while it was dominated by RISC of 2CzPN charge-transfer excitons at small ICs.

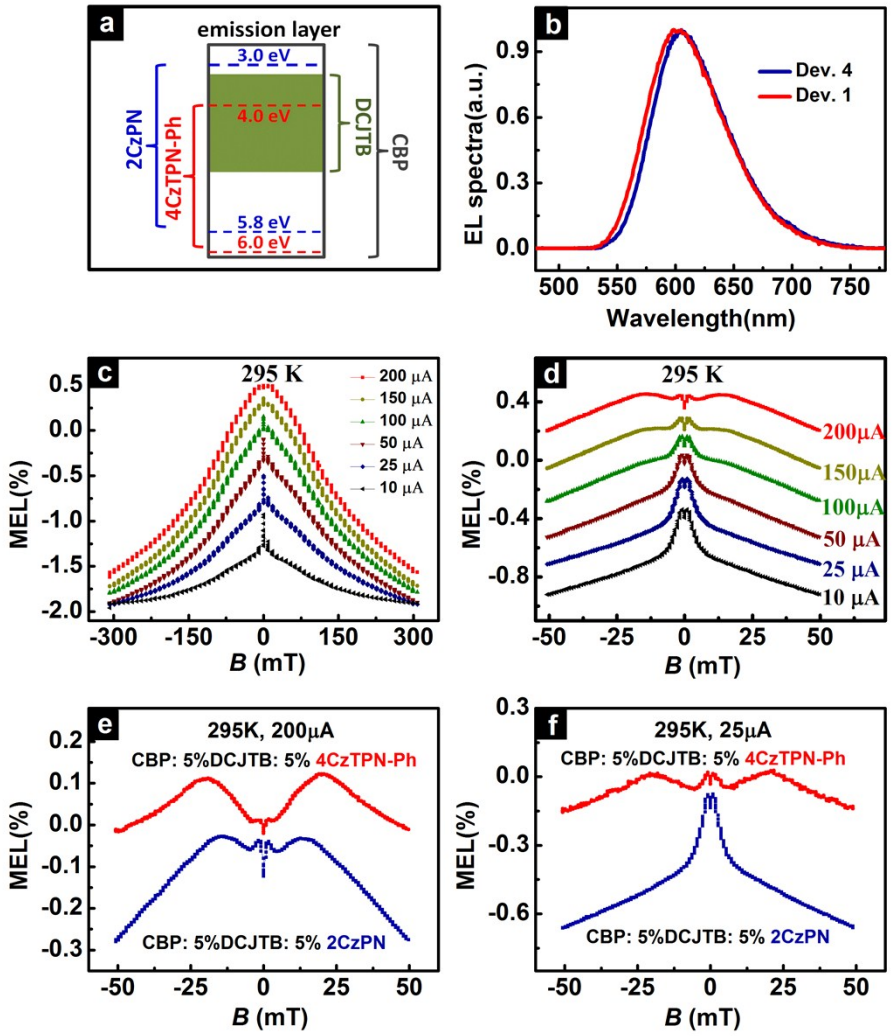

Fig. S5 (a) Energy levels of the emissive layer in Dev.1 and Dev.4. (b) Normalized EL spectra of Dev.1 and Dev.4. (c),(d) Current-dependent MEL(*B*) response of Dev.4 within a *B* of ±300 mT and ±50 mT at ambient temperature, respectively. In order to clearly see the MEL fine structures at the low field range, we fix the zero-field value of the MEL traces acquired at 50 μA to be zero, and vertically shift the corresponding MEL curves obtained at other currents, respectively. (e),(f) The MEL(*B*) response of Dev.1(red) and Dev.4 (blue) within a *B* of ±50 mT under large (200 uA) and small (25 uA) injection currents at ambient temperature, respectively. For the same reason, the zero-field values of the MEL traces of Dev.1 are fixed to be zero, and the MEL curves of Dev.4 are also vertically shifted.

As shown in Fig. S5d, the MEL curves from Dev.4 exhibited four components (MEL_{UL}, MEL_L, MEL_M, and MEL_H) at large currents (>150 μA), which was similar to the behaviors

observed from Dev.1 (Fig. 2d or 3a). However, the MEL curves from Dev.4 transformed from four components to three as the current was decreased. As mentioned, the line shapes of the MEL from Dev.4 and Dev.1 were generally similar, and so we can use the mechanisms determined for the four components of Dev.1 to analyze the MEL curves of Dev.4. Note that the relative contributions of these components in Dev.4 were different from those in Dev. 1. This indicated that the spin-pair state inter-conversions in the TADF-AF-OLEDs can be manipulated by controlling the efficiency of energy transfer between the TADF assisted sensitizer and the fluorescent dopant.

Specifically, the MEL curves from Dev.4 are compared with those from Dev.1 under large (200 μA) and small (25 μA) currents, as shown in Figs. S5e and S5f, respectively. By replacing 4CzTPN-Ph with a material with a larger energy gap (2CzPN), the energy transfer efficiency was improved. Thus, ISC of 2CzPN, RISC processes of DCJTB polaron pairs and 2CzPN charge-transfer excitons, and TF of DCJTB in Dev.4 were all enhanced when compared with Dev.1. This led to the observed increase in the MEL_{UL} component from Dev.4 because of the stronger ISC of 2CzPN compared with 4CzTPN-Ph. Additionally, the MEL_L component from Dev.4 was improved because of improved RISC of DCJTB polaron pairs and RISC of 2CzPN charge-transfer excitons. Moreover, the enhanced RISC of 2CzPN also led to the weakened MEL_M and the enhanced MEL_H at an IC of 25 μA. The enhanced TF of DCJTB in Dev.4 at 200 μA caused a larger decline in the MEL_H component.

Notes and references

1 T. D. Nguyen, T. P. Basel, Y. J. Pu, X. G. Li, E. Ehrenfreund and Z. V. Vardeny, *Phys. Rev. B,* 2012, **85**, 245437.

2 S. A. Crooker, F. Liu, M. R. Kelley, N. J. D. Martinez, W. Nie, A. Mohite, I. H. Nayyar, S. Tretiak, D. L. Smith and P. P. Ruden, *Appl. Phys. Lett.,* 2014, **105**, 153304.

3 Q. S. Zhang, B. Li, S. P. Huang, H. Nomura, H. Tanaka and C. Adachi, *Nat. Photon,*

2014, **8**, 326.

4 Q. M. Peng, W. J. Li, S. T. Zhang, P. Chen, F. Li and Y. G. Ma, *Adv. Opt. Mater.,* 2013, **1**, 362.

5 G. B. Piland, J. J. Burdett, D. Kurunthu and C. J. Bardeen, *J. Phys. Chem. C,* 2013, **117**, 1224.

6 P. Avakian and R. E. Merrifield, *Molecular Crystals.* 1968, **5**, 37.

7 P. Desai, P. Shakya, T. Kreouzis, W. P. Gillin, N. A. Morley and M. R. J. Gibbs, *Phys. Rev. B,* 2007, **75**, 094423.

8 A. A. Shoustikov, Y. J. You, and M. E. Thompson. *IEEE Journal of Selected Topics in Quantum Electronics*, 1998, **4**, 1.

9 Z. Y. Lu, Y. Hou, J. Xiao and H. S. Xu, Displays, 2014, **35**, 247.

10 X. Gong, H. Benmansour, G. C. Bazan and A. J. Heeger, *J. Phys. Chem. B*, 2006, **110**, 7344.

11 A. A. Shoustikov, Y. J. You and M. E. Thompson, *Abstracts of Papers of the American Chemical Society*, 1998, **215**, 526.

12 X. Gong, J. C. Ostrowski, D. Moses, G. C. Bazan, A. J. Heeger, *Advanced functional Materials*, 2003, **13**, 6.

13 P. Wang, S. L. Zhao, Z. Xu, B. Qiao, Z. J. Long and Q. Y. Huang, *Molecules*, 2016, **21**, 1365.

14 Y. Zhang, R. Liu, Y. L. Lei and Z. H. Xiong, *Appl. Phys. Lett.* 2009, **94**, 083307.

15 J. Kalinowski, M. Cocchi, D. Virgili, P. D. Marco and V. Fattori. *Chem. Phys. Lett.* 2003, **380**, 710.

16 Y. B. Chen, W. Y. Jia, J. Xiang, D. Yuan, Q. S. Chen, L. X. Chen, Z. H. Xiong. Identify triplet-charge interaction in rubrene-based diodes using magneto-conductance: Coexistence of dissociation and scattering channels. *Org. Electron.* **2016***, 39* 207.

17 T. D. Nguyen, T. P. Basel, Y. J. Pu, X. G. Li, E. Ehrenfreund and Z. V. Vardeny, *Phys.*

Rev. B, 2012, **85**, 245437.

18 P. Chen, Y. L. Lei, Q. L. Song, Y. Zhang, R. Liu, Q. M. Zhang and Z. H. Xiong. *Appl. Phys. Lett.,* 2009, **95**, 213304.